Citation for published version:

José R. Salgueiro and Albert Ferrando, "Energy- and time-controlled switching of ultrashort pulses in nonlinear directional plasmonic couplers," Opt. Lett. 47, 5136-5139 (2022), DOI https://doi.org/10.1364/OL.472269

Link to published version:
https://opg.optica.org/ol/fulltext.cfm?uri=ol-47-19-5136&id=507407

Energy and time controlled switching of ultrashort pulses in nonlinear directional plasmonic couplers

José R. Salgueiro[1,*] **and Albert Ferrando**[2,*]

[1] Universidade de Vigo, Escola de Enxeñaría Aeronáutica e do Espazo, As Lagoas s/n, 32004 Ourense, Spain
[2] Institut de Ciència dels Materiales, Universitat de València, C/ Catedràtic J. Beltran, 2, Paterna 46980, Spain
[*] Corresponding author: jrs@uvigo.es

Compiled December 26, 2022

We propose an ultra-compact nonlinear plasmonic directional coupler for switching of ultra-short optical pulses. We show that this device can be used to control the routing of ultra-short pulses using either the energy or the duration of each individual pulse as switching parameters. The coupler is composed of two cores of a nonlinear dielectric material embedded into metallic claddings. The intricate nonlinear spatiotemporal dynamics of the system is simulated by the Finite-Difference Time-Domain (FDTD) technique.

http://dx.doi.org/10.1364/ao.XX.XXXXXX

The interactions of electromagnetic radiation in metallic structures has come out to the field of plasmonics which has quickly developed great scientific and technological interest for nanophotonics. In fact, such structures containing metals are able to confine light to distances much shorter than wavelength —typically two orders of magnitude shorter— and to overpass the usual diffraction limits [1, 2]. This effect, which is extremely desirable to fabricate ultra-compact waveguiding devices[3–5], has, however, a serious drawback: it introduces an inherent high loss at optical frequencies inasmuch as metals do not behave as perfect conductors for the infrared or visible range of the spectrum. Nevertheless, in a nanometric scale these losses may become an acceptable inconvenience, balanced by the advantages described above, and so the achievement of functional devices results in a real possibility[6].

On the other hand, strong confinement at nanometric scales naturally induces extremely high intensities that cannot be ignored in the design of nanometric plasmonic waveguiding devices with dielectric cores. For this reason, in the analysis of ultra-compact plasmonic devices with light confined in dielectric cores with a typical width one order of magnitude smaller than the carrier wavelength, nonlinear effects are expected to play a crucial role and they should be considered in the design process. On the other hand, additional functionalities are expected to come to light from the use of nonlinear effects to carry out all-optical processing of signals. In fact, different nonlinear plasmonic devices were already described[7–9] as slot waveguides or directional couplers and functional systems demonstrated for optical limiting, self-phase modulation, second harmonic generation or logic gates. The best studied devices operate, however, in a CW regime.

The possibility of using ultrashort pulses increasing the power density is definitively an advantage to efficiently triggering the nonlinear response with a reasonable amount of energy. Modeling such systems is more difficult, however, as nonlinear spatiotemporal effects come into play, specially in highly dispersive materials as metals. Nonlinear plasmonic systems with ultrashort pulses are in such a way little studied. Only few works can be found where plasmonics is combined with short pulses, mainly focused on simple devices as surface plasmon polaritons (SPP) in metal-dielectric interfaces[10–16] or single slot waveguides [17, 18].

In this work we study switching by ultrashort pulses in a two slot waveguide plasmonic directional coupler, simulating the system by the finite-difference time-domain (FDTD) technique. In the following we will then describe the system as well as the way to model its metal and nonlinear dielectric layers. Section describes the linear regime and the evaluation of the coupler beating length discussing its dependence on the pulse timewidth. Then two studies on the device as an optical switch will be carried out, one based on pulse energy and the other on pulse duration.

The device is formed by two parallel identical planar waveguides with dielectric nonlinear cores embedded in metallic claddings. In Fig. 1 a sketch of the structure is shown and its expected behavior for pulse multiplexing illustrated. The structure lies in the XZ plane being invariant in the y-direction. Coordinates x and z describe transversal and propagation directions respectively and they both are normalized after rescaling by the wavenumber $k_0 = \omega_0/c = 2\pi/\lambda_0$ at a particular reference wavelength λ_0 (c is the vacuum speed of light). Time is also scaled to normalized units using the correspondent reference frequency $\omega_0 = 2\pi c/\lambda_0$. We chose $\lambda_0 = 800\,\mathrm{nm}$ meaning a space normalized unit of about 127 nm and a normalized time unit of 0.42 fs. Fields are also expressed in Heaviside-Lorentz units in order to drop all the natural constants in Maxwell equations and make both electric and magnetic fields to have a similar scale. We consider a TE-polarized field —TM in the waveguiding theory context— with in plane electric components E_x and E_z and a perpendicular to the plane magnetic component H_y.

As it was shown in other nonlinear systems based on directional couplers[19], for a CW beam there is a change of regime from linear to nonlinear as power increases. For a pulse such

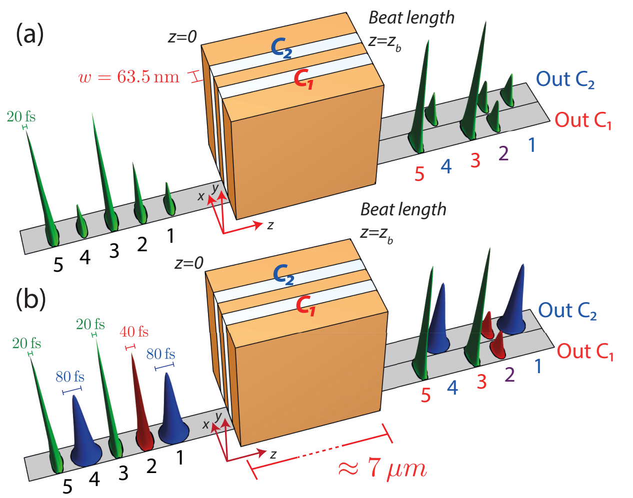

Fig. 1. Sketch of the directional coupler with the reference system. Clear zones are waveguide cores while dark zones are metallic claddings. (a) Illustration of the device use for pulse-energy multiplexing. (b) Intended use for pulse time-width multiplexing.

effect is also expected and related to the energy and time-width as both parameters determine its power density profile. If both waveguides are identical, in a linear regime energy is transferred from one core to the other after propagation for a so-called beating length. In a nonlinear regime, however, propagation for such a distance makes energy to partially remain in the same core to which it was originally coupled.

Considering a device of a beating length, pulses of different energy but same time-width are expected to switch from the second core to the first one as energy increases [Fig.1(a)], i.e. the low energy ones are transferred to the second core remaining at the first core those with higher energy. On the other hand, for pulses of different time-width but same energy it is expected a transference of the long ones, remaining the short ones at the first core [Fig.1(b)]. In an intermediate regime a mixed behavior should be obtained. This setup of a beating length constitutes the functional part of the device and a practical implementation would require from input waveguides which get closer and connect to the coupler as well as output waveguides which separate away from the coupler.

The device is simulated using the FDTD technique describing both cores and claddings with a specific model. Nonlinear cores are suppose to show a Kerr response with dielectric function $\epsilon = \epsilon_l + \alpha|\vec{E}|^2$, where ϵ_l is the linear dielectric constant and α the Kerr coefficient. The time domain modeling is accomplished assuming an instantaneous response [20] taken $\epsilon_l = 2.25$ and a normalized nonlinear coefficient $\alpha = 1$. This value only implies an appropriate rescaling of the field amplitude and has no qualitative influence. Consequently, the results are qualitatively valid for any nonlinear Kerr-type dielectric. Quantitative results only require the use of the particular dielectric constant ϵ_l and the rescaling of the field with the particular Kerr coefficient α.

In order to model the metallic claddings a cold plasma model was considered[20] described by the Drude formula,

$$\epsilon(\omega) = 1 - \frac{\omega_p^2}{\omega^2 + i\Gamma\omega}, \tag{1}$$

dependent on two parameters, the plasma frequency ω_p and the electronic collision frequency Γ. We took silver as the cladding metal and so those parameters were evaluated from experimental data taken from the literature[21] at the chosen reference frequency $\omega_0 = 2\pi c/\lambda_0$, obtaining the values $\omega_p = 1.30 \times 10^{16}$ Hz and $\Gamma = 2.93 \times 10^{13}$ Hz. Nonlinear response of the metal was not taken into account for simplicity. Nevertheless there are studies claiming that the nonlinear response of metals could be as important as that of many dielectrics[22, 23] and so a more elaborated model could be necessary in future for a more accurate description[24]. In any case, this linear model is expected to be realistic when the dielectric used for the cores presents a strongly enough nonlinearity, well over the metal nonlinearities.

The FDTD modeling[20] is carried out dividing the structure into different domains and using the specific model for the corresponding material. Also specific models to implement the Perfect Matching Layers (PML) are used at the domains surrounding the structure (Fig. 1) to get rid of the radiation that reaches the boundaries. On the other hand, a source is implemented at the line $z = 0$ correspondent to one of the cores (first core) using the total-field/scattered-field (TF/SF) technique. Since the system is nonlinear, it is relevant the amount of energy forward-coupled into the waveguide and so this technique is useful to minimize the back-reflected energy.

Following previous experience modeling this type of devices[19, 25] we chose cores of width $w = 0.5$ separated by a distance of $d = 0.5$. For the given values, as it will be found in section , beating length is around $z_b \sim 50$. This means the device will have transversal dimensions of about 350 nm, well into the nanoscale, and a longitudinal dimension of about 7 μm, reasonably small to keep losses to acceptable values.

The first study was carried out in linear regime to determine the beating length of the coupler, i.e. the necessary propagation distance to transfer all the energy to the second core. The Kerr coefficient was consequently set as $\alpha = 0$ and a pulse of Gaussian spatial as well as temporal shape was launched into the input (first) core (C_1 in Fig. 1). The total energy of the pulse for any of the cores is obtained at each z-position by the time-integration of the power flux, i.e. integrating the z-component of the Poynting vector in space (limited to the half-plane correspondent to each core) and time:

$$W_{1,2}(z) = \int_0^{t_f} \int_{C_{1,2}} \left[\vec{S}(x,z) \cdot \hat{z}\right] dx dt, \tag{2}$$

where integration domains for cores C_1 and C_2 are respectively $C_1 \equiv [-\infty, 0)$ and $C_2 \equiv (0, +\infty]$ and time t_f stands for the total simulation time. In Fig. 2 we plot the results for three different values of the pulse time-width (Δt) including results for a loseless medium [i.e. taken $\Gamma = 0$ in Eq. (1)] for the sake of comparison.

Losses are responsible for the mismatch between the minima and maxima of both curves (Fig. 2) in the lossy case. The beating length changes very little with pulse duration (Δt) and may be considered independent of it except but for the lowest values of Δt. Additionally, for shortest pulses (case $\Delta t = 5$ in Fig. 2), there is not a complete transfer of energy to the second core in a coupling cycle and the accumulated effect in a number of cycles lead to a balanced energy distribution at both cores.

Simulations in nonlinear regime were carried out launching pulses into the first core and measuring the energy propagating to a beating length. Energy evaluation was done integrating the power at the ouput $z = z_b$, as described in Sec. and comes given by Eq. (2). For this study pulse time-width was kept constant

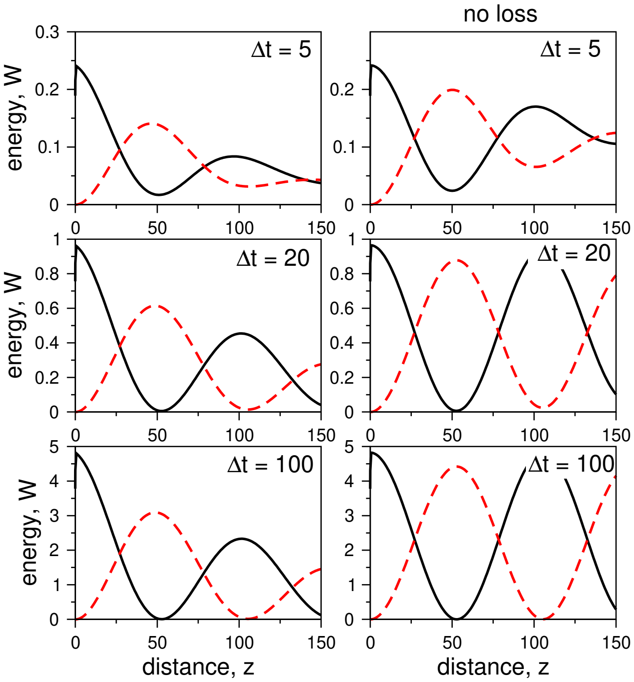

Fig. 2. Energy (accumulated power) crossing at position z for every half-plane related to each of the cores. Continuous and thin dashed lines are respectively energies for core C_1 (the excited one) and core C_2. Rows are results for different pulse duration Δt as indicated. Both columns show results for the realistic (left column) and non lossy (right column) case respectively.

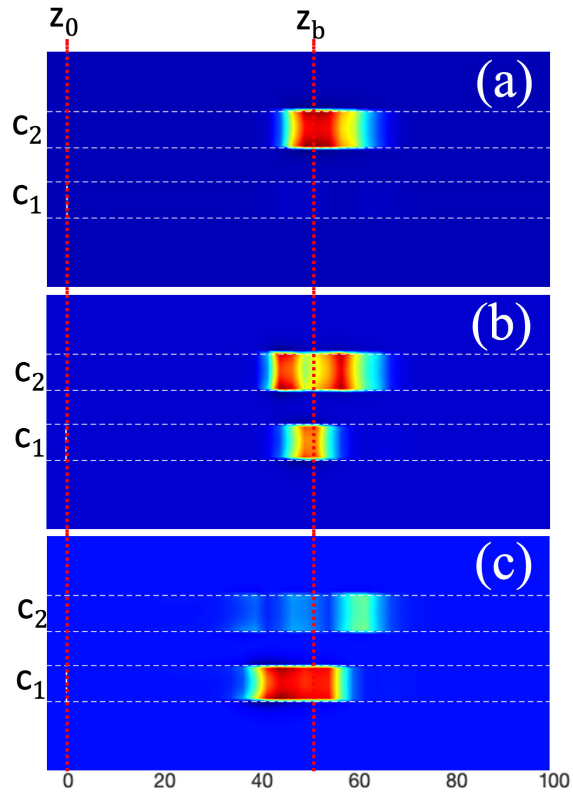

Fig. 3. Three simulations of pulse coupling for three different values of input energy. They correspond to a linear (a), intermediate (b) and fully nonlinear (c) regimes. Simulations are for a non lossy case ($\Gamma = 0$) and for an input pulse-width $\Delta t = 20$. Vertical dashed lines mark the source ($z = 0$), and beating length ($z = z_b$) positions.

so that its energy is directly related to amplitude. In Fig. 3 an example showing the three main scenarios is presented: linear regime (a), intermediate (b) and nonlinear (c) and illustrating the change of state of the coupler as energy rises.

In Fig. 4 we present plots of the measured energy at the beating length position $z = z_b$, normalized by the input energy, against the input energy. Both realistic and non lossy cases are presented for the sake of comparison and the different curves on each of the plots correspond to different input pulse time-width. Vertical scale is mainly conditioned by the loss and is an indicative of the coupler efficiency. The curves show the change of state (switching) as pulse energy overpass a particular threshold.

Along with efficiency other relevant characteristics are switching sharpness and switching sensitivity. Sharpness is determined by the slope of the curve when the change of regime takes place. In Fig. 4 it is shown such slope increases as pulse time-width decreases, leading to a sharper transition for shorter pulses. On the other hand sensitivity refers to the energy threshold to induce the change of state. In the figure it is shown how shorter pulses trigger the change of state at lower energy revealing a higher sensitivity for short pulses. This means the use of short pulses constitute a definitive advantage respect to long pulses or CW beams.

The dependence of the switching threshold on pulse duration suggest the possibility of carrying out another switching modality based on pulse time-width for fixed-energy pulses. In Fig. 5 normalized output energy is plotted against input pulse-width for three different input energy values. For short pulses power density is larger and nonlinearity drives the process making a larger amount of energy to remain at the excited core. As pulses get longer the nonlinear response gets weaker and a greater amount of energy transfers to the second core (dashed lines), decreasing in the first one (the excited one) to almost zero (continuous lines). High energy pulses require a longer duration to trigger the change of state. In Fig. 6 plots of the input and output power flux against time are presented for three different values of the input pulse-width to better illustrate this change. The output pulses at each core show the transition from a balanced output between cores (short pulses) to a full energy transfer to the second core (long pulses) resulting a pulse-routing effect as was initially expected.

In conclusion, simulations of pulse propagation in plasmonic directional couplers were carried out both in linear and nonlinear regimes. In linear regime it was shown there is little dependence of the beating length to the pulse duration except but for the shortest pulses. In nonlinear regime switching was demonstrated for fixed time-width pulses when pulse energy is raised, as well as for fixed energy pulses when pulse duration is changed. Switching sharpness as well as sensitivity increase for shorter pulses. The studied effects are useful for pulse discrimination and allow pulse routing according to their energy or time-width.

Funding. We thank the support of MCIN of Spain through the project PID2020-120484RB-I00, as well as Xunta de Galicia, Spain (grant ED431B 2021/22) and Generalitat Valenciana, Spain (grant PROMETEO/2021/082).

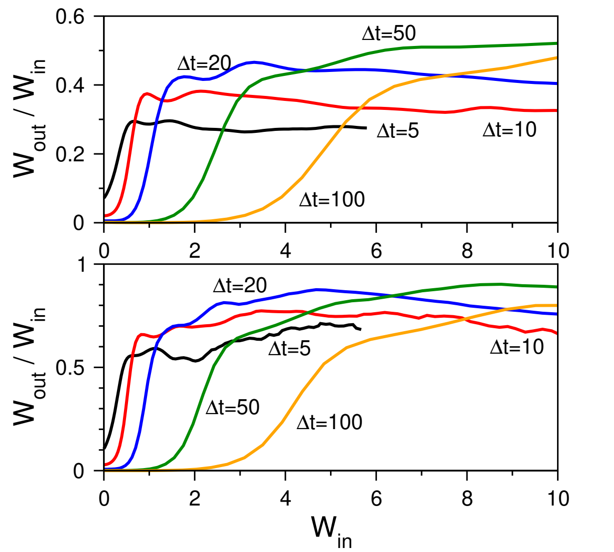

Fig. 4. Switching curves for different values of the pulse time-width Δt as indicated on the curve labels. W_{in} and W_{out} stand for input and output energy at core C_1. Curves show normalized output energy against input energy. Both realistic (top) and non lossy (bottom) cases are shown.

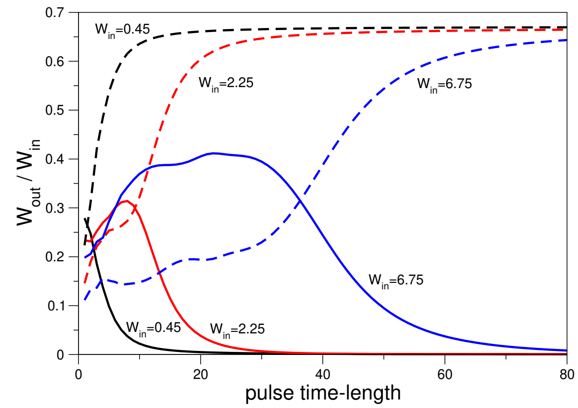

Fig. 5. Normalized output energy against input pulse time-width Δt for three different pulse input-energy values as indicated on the labels. The input pulse is launched into the first core (C_1). Continuous and dashed lines refer to the output at the first (C_1) and second (C_2) core respectively.

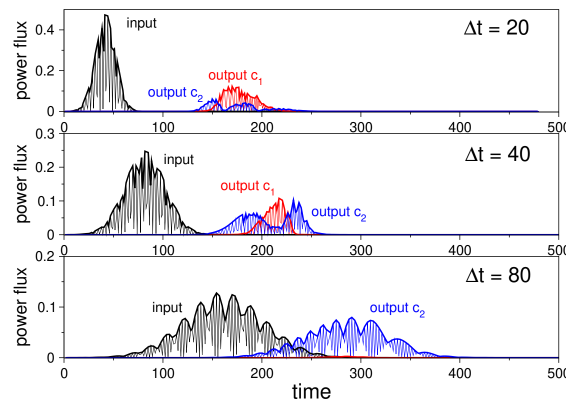

Fig. 6. Power flux against time at input position (core C_1) and both core outputs. Pulse-energy is fixed to $W_{in} = 6.75$ and each subplot correspond to a different input pulse time-width as indicated.

Disclosures. The authors declare no conflicts of interest.

REFERENCES

1. W. L. Barnes, A. Dereux, and T. W. Ebbesen, Nature **424**, 824 (2003).
2. S. I. Bozhevolnyi, V. S. Volkov, E. Devaux, J. Y. Laluet, and T. W. Ebbesen, Nature **440**, 508 (2006).
3. A. Degiron, S. Y. Cho, T. Tyler, N. M. Jokerst, and D. R. Smith, New J. Phys. **11**, 015002 (2009).
4. T. Holmgaard, Z. Chen, S. I. Bozhevolnyi, L. Markey, and A. Dereux, J. Light. Technol. **27**, 5521 (2009).
5. A. Dolatabady and N. Granpayeh, Plasmonics **12**, 597 (2017).
6. F. Lou, Z. Wang, D. Dai, L. Thylen, and L. Wosinski, App. Phys. Lett. **100**, 242205 (2012).
7. A. Tuniz, La Rivista del Nuovo Cimento **44**, 193 (2021).
8. N. C. Panoiu, W. E. I. Sha, D. Y. Lei, and G.-C. Li, J. Opt. **20**, 083001 (2018).
9. M. Kauranen and A. V. Zayats, Nat. Photonics **6**, 737 (2012).
10. K. F. MacDonald, Z. L. Sámson, M. I. Stockman, and N. I. Zheludev, Nat. Photonics **3**, 55 (2009).
11. Z. L. Sámson, P. Horak, K. F. MacDonald, and N. I. Zheludev, Opt. Lett. **36**, 250 (2011).
12. N. Nozhat and N. Granpayeh, Opt. Commun. **285**, 1555 (2012).
13. D. O. Ignatyeva and A. P. Sukhorukov, Phys. Rev. A **013850** (2014).
14. N. Khokhlov, D. Ignatyeva, and V. Belotelov, Opt Express **22**, 28019 (2014).
15. M. Klein, B. H. Badada, R. Binder, A. Alfrey, M. McKie, M. R. Koehler, D. G. Mandrus, T. Taniguchi, K. Watanabe, B. J. LeRoy, and J. R. Schaibley, Nat. Commun. **1**, 3264 (2019).
16. I. V. Dzedolik and A. Y. Leksin, J. Opt. **22**, 075001 (2020).
17. A. Pusch, I. V. Shadrivov, O. Hess, and Y. S. Kivshar, Opt. Express **21**, 1121 (2013).
18. O. Lysenko, M. Bache, N. Olivier, A. V. Zayats, and A. Lavrinenko, ACS Photonics **3**, 2324 (2020).
19. J. R. Salgueiro and Y. S. Kivshar, Appl. Phys. Lett. **97**, 081106 (2010).
20. A. Taflove, *Computational electrodynamics, the finite difference time domain* (Artech House Publishers, Norwood, Massachussets, 2005).
21. P. B. Johnson and R. W. Christy, Phys. Rev. B **6**, 4370 (1972).
22. P. Ginzburg, A. Hayat, N. Berkovitch, and M. Orenstein, Opt. Lett. **35**, 1551 (2010).
23. A. V. Krasavin, P. Ginzburg, and A. V. Zayats, Laser & Photonics Rev. **12**, 1700082 (2018).
24. A. Marini, M. Conforti, G. Della Valle, H. W. Lee, T. X. Tran, W. Chang, M. A. Schmidt, S. Longhi, P. St J Russell, and F. Biancalana, New J. Phys. **15**, 013033 (2013).
25. J. R. Salgueiro and Y. S. Kivshar, J. Opt. **16**, 1 (2014).

FULL REFERENCES

1. W. L. Barnes, A. Dereux, and T. W. Ebbesen, “Surface plasmon subwavelength optics,” Nature **424**, 824–830 (2003).
2. S. I. Bozhevolnyi, V. S. Volkov, E. Devaux, J. Y. Laluet, and T. W. Ebbesen, “Channel plasmon subwavelength waveguide components including interferometers and ring resonators,” Nature **440**, 508–511 (2006).
3. A. Degiron, S. Y. Cho, T. Tyler, N. M. Jokerst, and D. R. Smith, “Directional coupling between dielectric and long-range plasmon waveguides,” New J. Phys. **11**, 015002 (2009).
4. T. Holmgaard, Z. Chen, S. I. Bozhevolnyi, L. Markey, and A. Dereux, “Design and characterization of dielectric-loaded plasmonic directional couplers,” J. Light. Technol. **27**, 5521–5528 (2009).
5. A. Dolatabady and N. Granpayeh, “Plasmonic directional couplers based on multi-slit waveguides,” Plasmonics **12**, 597–604 (2017).
6. F. Lou, Z. Wang, D. Dai, L. Thylen, and L. Wosinski, “Experimental demonstration of ultra-compact directional couplers based on silicon hybrid plasmonic waveguides,” App. Phys. Lett. **100**, 242205 (2012).
7. A. Tuniz, “Nanoscale nonlinear plasmonics in photonic waveguides and circuits,” La Rivista del Nuovo Cimento **44**, 193–249 (2021).
8. N. C. Panoiu, W. E. I. Sha, D. Y. Lei, and G.-C. Li, “Nonlinear optics in plasmonic nanostructures,” J. Opt. **20**, 083001 (2018).
9. M. Kauranen and A. V. Zayats, “Nonlinear plasmonics,” Nat. Photonics **6**, 737–748 (2012).
10. K. F. MacDonald, Z. L. Sámson, M. I. Stockman, and N. I. Zheludev, “Ultrafast active plasmonics,” Nat. Photonics **3**, 55–58 (2009).
11. Z. L. Sámson, P. Horak, K. F. MacDonald, and N. I. Zheludev, “Femtosecond surface plasmon pulse propagation,” Opt. Lett. **36**, 250–252 (2011).
12. N. Nozhat and N. Granpayeh, “Switching power reduction in the ultracompact kerr nonlinear plasmonic directional coupler,” Opt. Commun. **285**, 1555–1559 (2012).
13. D. O. Ignatyeva and A. P. Sukhorukov, “Femtosecond-pulse control in nonlinear plasmonic systems,” Phys. Rev. A **013850** (2014).
14. N. Khokhlov, D. Ignatyeva, and V. Belotelov, “Plasmonic pulse shaping and velocity control via photoexcitation of electrons in a gold film.” Opt Express **22**, 28019–28026 (2014).
15. M. Klein, B. H. Badada, R. Binder, A. Alfrey, M. McKie, M. R. Koehler, D. G. Mandrus, T. Taniguchi, K. Watanabe, B. J. LeRoy, and J. R. Schaibley, “2d semiconductor nonlinear plasmonic modulators,” Nat. Commun. **1**, 3264 (2019).
16. I. V. Dzedolik and A. Y. Leksin, “Controlled flow of nonlinear surface plasmon polaritons,” J. Opt. **22**, 075001 (2020).
17. A. Pusch, I. V. Shadrivov, O. Hess, and Y. S. Kivshar, “Self-focusing of femtosecond surface plasmon polaritons,” Opt. Express **21**, 1121–1127 (2013).
18. O. Lysenko, M. Bache, N. Olivier, A. V. Zayats, and A. Lavrinenko, “Nonlinear dynamics of ultrashort long-range surface plasmon polariton pulses in gold strip waveguides,” ACS Photonics **3**, 2324–2329 (2020).
19. J. R. Salgueiro and Y. S. Kivshar, “Nonlinear plasmonic directional couplers,” Appl. Phys. Lett. **97**, 081106 (2010).
20. A. Taflove, *Computational electrodynamics, the finite difference time domain* (Artech House Publishers, Norwood, Massachussets, 2005).
21. P. B. Johnson and R. W. Christy, “Optical constants of the noble metals,” Phys. Rev. B **6**, 4370–4379 (1972).
22. P. Ginzburg, A. Hayat, N. Berkovitch, and M. Orenstein, “Nonlocal ponderomotive nonlinearity in plasmonics,” Opt. Lett. **35**, 1551–1553 (2010).
23. A. V. Krasavin, P. Ginzburg, and A. V. Zayats, “Free-electron optical nonlinearities in plasmonic nanostructures: A review of the hydrodynamic description,” Laser & Photonics Rev. **12**, 1700082 (2018).
24. A. Marini, M. Conforti, G. Della Valle, H. W. Lee, T. X. Tran, W. Chang, M. A. Schmidt, S. Longhi, P. St J Russell, and F. Biancalana, “Ultrafast nonlinear dynamics of surface plasmon polaritons in gold nanowires due to the intrinsic nonlinearity of metals,” New J. Phys. **15**, 013033 (2013).
25. J. R. Salgueiro and Y. S. Kivshar, “Complex modes in plasmonic nonlinear slot waveguides,” J. Opt. **16**, 1–10 (2014).